

## Electronic Supplementary Information

### Experimental section

**Materials:** Oxalic acid ( $\text{H}_2\text{C}_2\text{O}_4$ , 99.0%), sodium nitrite ( $\text{NaNO}_2$ ), sodium dihydrogen phosphate dihydrate ( $\text{Na}_2\text{HPO}_4 \cdot 2\text{H}_2\text{O}$ ), sodium phosphate dibasic dodecahydrate ( $\text{NaH}_2\text{PO}_4 \cdot 12\text{H}_2\text{O}$ ), ammonium chloride ( $\text{NH}_4\text{Cl}$ ), sodium hydroxide ( $\text{NaOH}$ ), salicylic acid ( $\text{C}_7\text{H}_6\text{O}_3$ ), sodium citrate dihydrate ( $\text{C}_6\text{H}_5\text{Na}_3\text{O}_7 \cdot 2\text{H}_2\text{O}$ ), p-dimethylaminobenzaldehyde ( $\text{C}_9\text{H}_{11}\text{NO}$ ), sodium nitroferricyanide dihydrate ( $\text{C}_5\text{FeN}_6\text{Na}_2\text{O} \cdot 2\text{H}_2\text{O}$ ), and sodium hypochlorite solution ( $\text{NaClO}$ ) were purchased from Chengdu Kelong Co., Ltd. All reagents were used directly without further purification. Copper foil was purchased from Suzhou Yilongsheng Energy Technology Co., Ltd.

**Preparation of CF@Cu<sub>2</sub>O and CF@Cu<sub>2</sub>O-1:** CF@Cu<sub>2</sub>O was prepared as follows: first, a piece of copper foil ( $1 \times 2 \text{ cm}^2$ ) was cleaned ultrasonically in 3 M HCl solution for 2 minutes. Then the sample was rinsed with deionized water for several times and dried under ambient conditions for further use. Anodic oxidation was carried out in 0.5 M oxalic acid solution at 5 V for 5 minutes with a pretreated copper foil as the positive electrode and a platinum plate as the negative electrode. The oxidized copper foil was cleaned with deionized water and annealed at 550 °C for 1 h under Ar atmosphere. To prepare CF@Cu<sub>2</sub>O-1 with small oxygen vacancy concentration, a piece of CF@Cu<sub>2</sub>O was further annealed at 200 °C in air for 12h.

**Characterization:** XRD data were determined using X-ray diffractometer with Cu K $\alpha$  radiation (DX-2700B). SEM measurements were carried out on a field-emission

scanning electron microscopy (FEI Insect F50). TEM images were obtained using an atomic-resolution scanning transmission electron microscopy (FEI Talos F200S Super). XPS measurements were performed with Thermo Fischer ESCALAB Xi<sup>+</sup>. The absorbance data were measured by an ultraviolet-visible spectrophotometer. The pH value of the electrolyte is measured with a Rayman PHSJ-6L type pH meter.

***Electrochemical measurements:*** All electrochemical measurements were carried out in an H-shaped electrochemical cell separated by Nafion membrane using CHI 660E electrochemical workstation (Chenhua, Shanghai). CF@Cu<sub>2</sub>O, Ag/AgCl, and graphite rod were used as working electrode, reference electrode, and reference electrode, respectively. The area of the working electrode immerse in electrolyte is 0.25 cm<sup>2</sup>. LSV was performed in Ar-saturated 0.1 M PBS with 0.1 M NaNO<sub>2</sub> at a scan rate of 5 mV s<sup>-1</sup>. All potentials reported in this work were converted to reversible hydrogen electrode (RHE) scale and current densities were normalized to the geometric surface area.

***Determination of NH<sub>3</sub>:*** The NH<sub>3</sub> concentration in the solution was determined (the obtained electrolyte was diluted 50 times) by the indophenol blue method.<sup>1</sup> In detail, 2 mL of coloring solution (1 M NaOH containing 5% salicylic acid and 5% sodium citrate), 1 mL of oxidizing solution (0.05 M NaClO), and 0.2 mL of catalyst solution (1 wt% C<sub>5</sub>FeN<sub>6</sub>Na<sub>2</sub>O·2H<sub>2</sub>O) were added to 2 mL of the electrolyte after electrolysis. After standing for 2 h in the dark, the UV-Vis absorption spectra were measured. The concentration of NH<sub>3</sub> was identified using absorbance at a wavelength of 655 nm. The concentration-absorbance curve was calibrated using the standard NH<sub>4</sub>Cl solution

with known concentrations of 0.0, 0.25, 0.5, 1.0, 1.5, and 2  $\mu\text{g mL}^{-1}$  in 0.1 M PBS. The fitting curve ( $y = 0.43158x + 0.06198$ ,  $R^2 = 0.99986$ ) shows good linear relation of absorbance value with  $\text{NH}_3$  concentration.

***Determination of  $\text{NH}_3$  FE and yield rate:***

The  $\text{NH}_3$  FE is estimated from the charge consumed for  $\text{NO}_2^-$  reduction and total charge pass through the electrode:

$$\text{FE} = 6FC_{\text{NH}_3}V / (M_{\text{NH}_3}Q)$$

The yield rate of  $\text{NH}_3$  (aq) is calculated:

$$\text{Yield rate} = C_{\text{NH}_3}V / (M_{\text{NH}_3}tA)$$

Where  $C_{\text{NH}_3}$  is the concentration of  $\text{NH}_3$  (aq), F is the Faradaic constant (96485 C  $\text{mol}^{-1}$ ), V is the volume of electrolyte in the anode compartment (45 mL),  $M_{\text{NH}_3}$  is the molar mass of  $\text{NH}_3$ , Q is the total charge passing the electrode, t is the electrolysis time, and A is the geometric surface area.

***DFT theoretical calculation:***

First-principles calculations with spin-polarized were performed based on DFT implemented in the VASP package,<sup>2, 3</sup> and the interaction between valence electrons and ionic core were expanded using the projector augmented wave (PAW) approach with a cutoff of 450 eV. Perdew-Burke-Ernzerhof functional (PBE)<sup>4, 5</sup> with semi-empirical corrections of DFT-D3 was adopted to describe exchange-correlation functional effect based on general gradient approximation (GGA).<sup>6, 7</sup> We modeled the catalyst using pristine  $\text{Cu}_2\text{O}$  (111) surface, with one OV and Cu (111) surface in four layers, for which the bottom two layer was fixed and the upper two layers were

allowed to relax. The thickness of the vacuum region is  $>15 \text{ \AA}$  to avoid the spurious interaction. The Brillouin zone was sampled by  $3 \times 5 \times 1$  and  $3 \times 3 \times 1$  special k-points using the Monkhorst Pack scheme for structural configuration optimization of  $\text{Cu}_2\text{O}$  (111) and Cu (111), respectively. The force convergence thresholds are  $0.02 \text{ eV/\AA}$  and the total energy less than  $1\text{E-}5 \text{ eV}$ , respectively. The theoretical calculation results were processing and analyzed by VASPKIT software.<sup>8</sup>

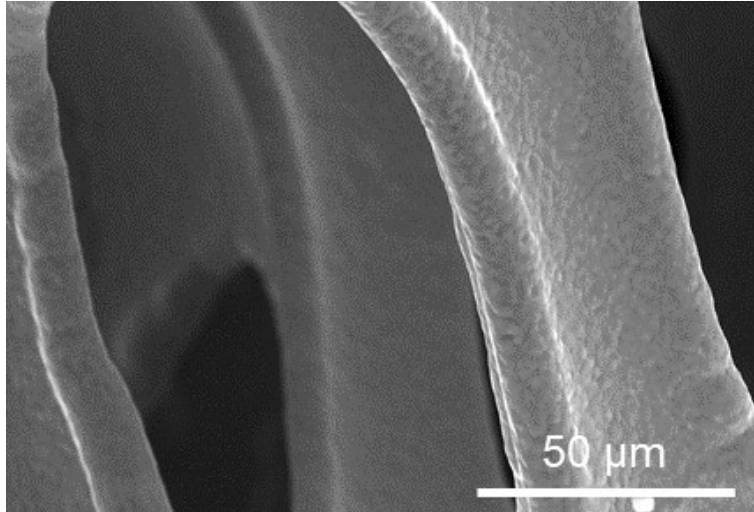


**Fig. S1** SEM image of Cu foam.

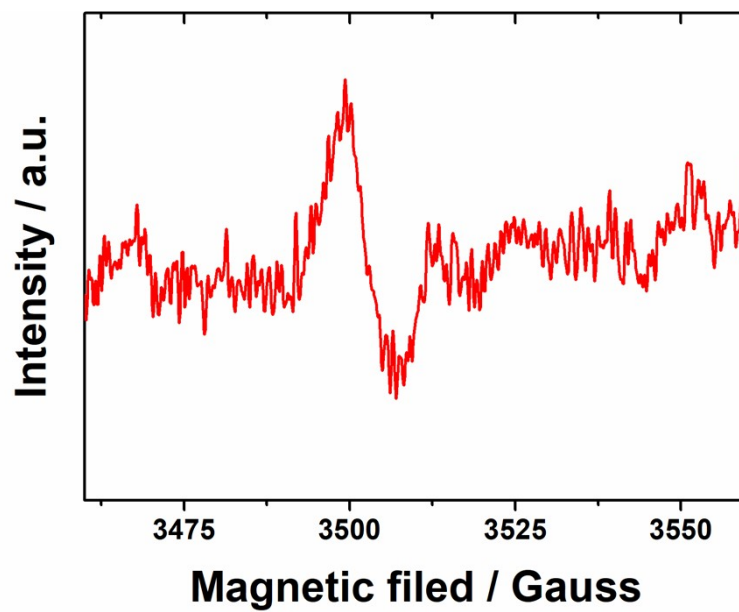


**Fig. S2** ESR spectrum of CF@Cu<sub>2</sub>O.

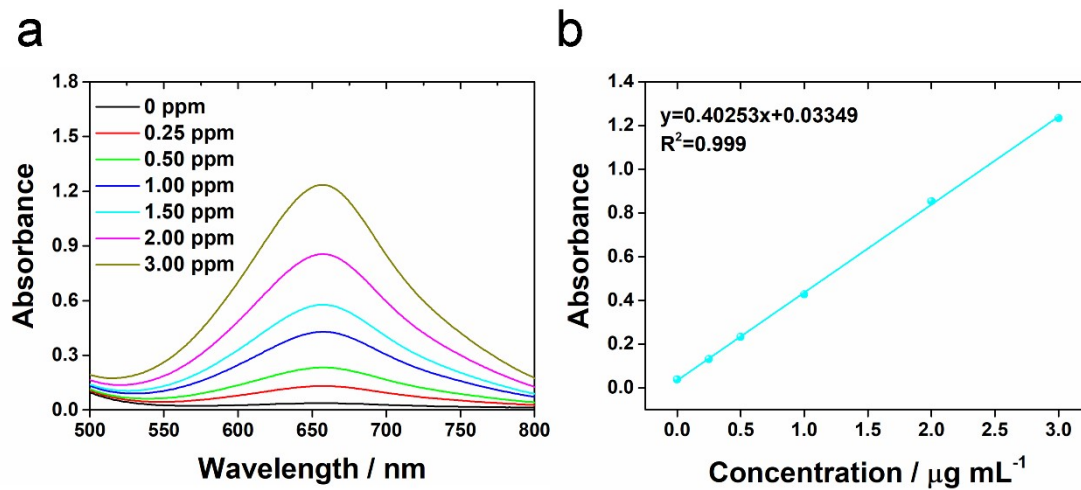


**Fig. S3** (a) UV-Vis spectra and (b) corresponding calibration curve used for calculation of  $\text{NH}_4^+$  concentration.

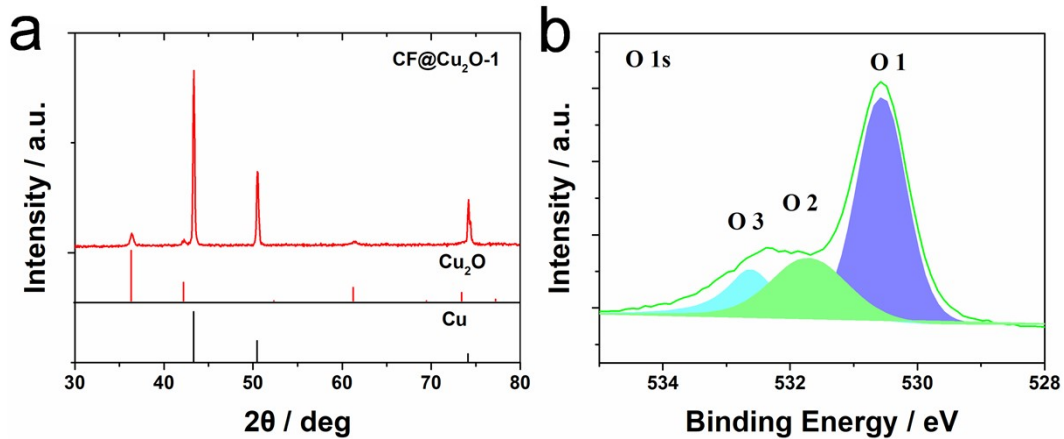


**Fig. S4** (a) XRD pattern and (b) XPS spectrum of O 1s region for CF@Cu<sub>2</sub>O-1.

After further calcination of CF@Cu<sub>2</sub>O at 200°C in air for 12 h, the obtained CF@Cu<sub>2</sub>O-1 also shows a XRD pattern corresponding to Cu<sub>2</sub>O (Fig. S4a). In O 1s region (Fig. S4b), the peak area of O2 at 531.7 eV is obviously smaller than that of CF@Cu<sub>2</sub>O (Fig. 2i), implying a small oxygen vacancy concentration of CF@Cu<sub>2</sub>O-1.

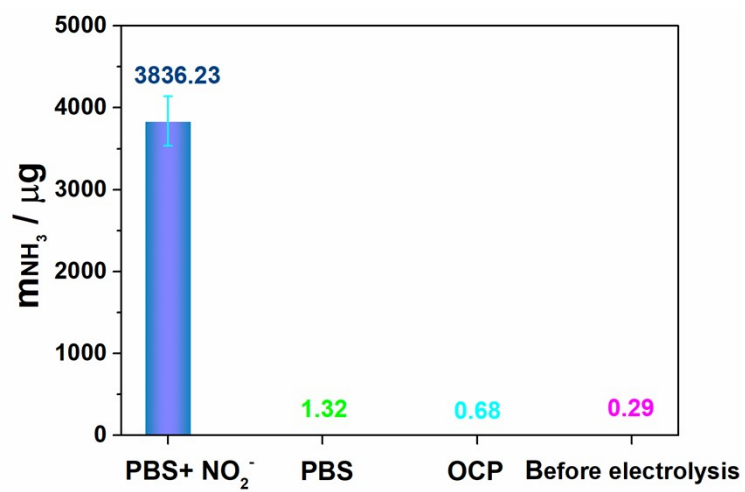


**Fig. S5** Amounts of produced  $\text{NH}_3$  under different conditions.

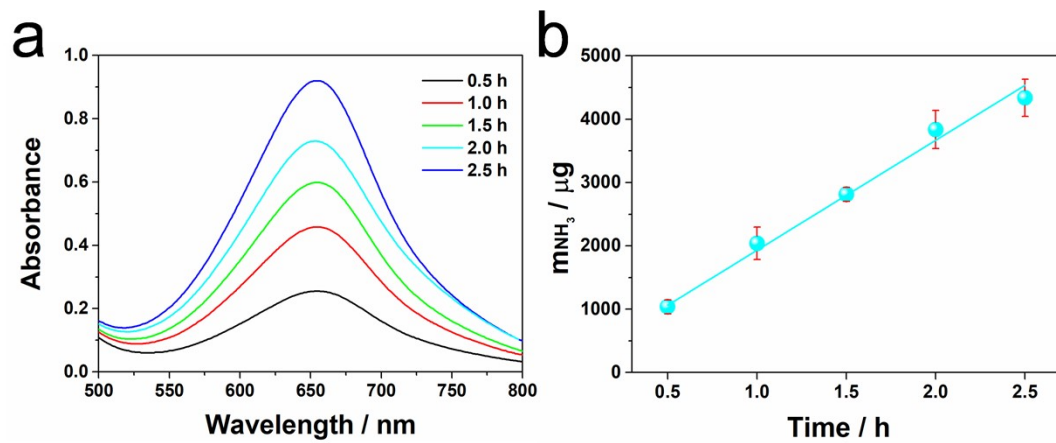


**Fig. S6** (a) UV-vis spectra and (b) NH<sub>3</sub> yields of CF@Cu<sub>2</sub>O at different electrolysis time.

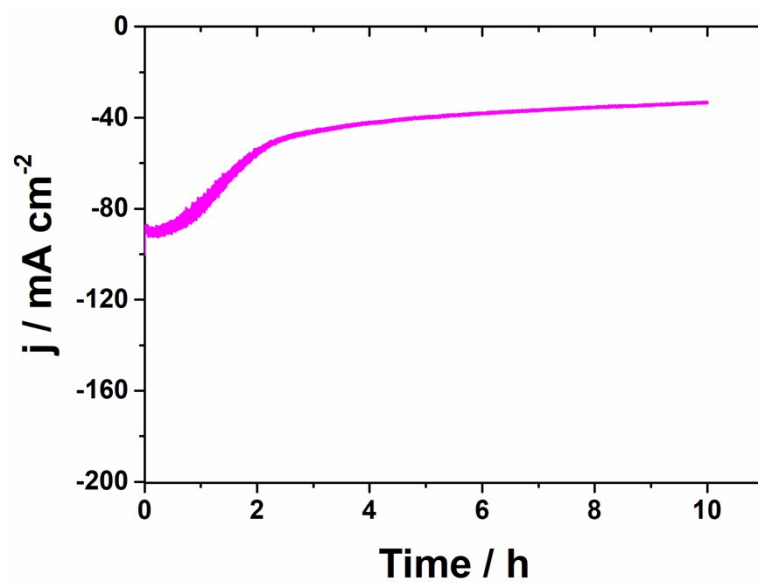


**Fig. S7** Chronoamperometric curve of CF@Cu<sub>2</sub>O for NO<sub>2</sub><sup>-</sup>RR at -0.6 V vs RHE.

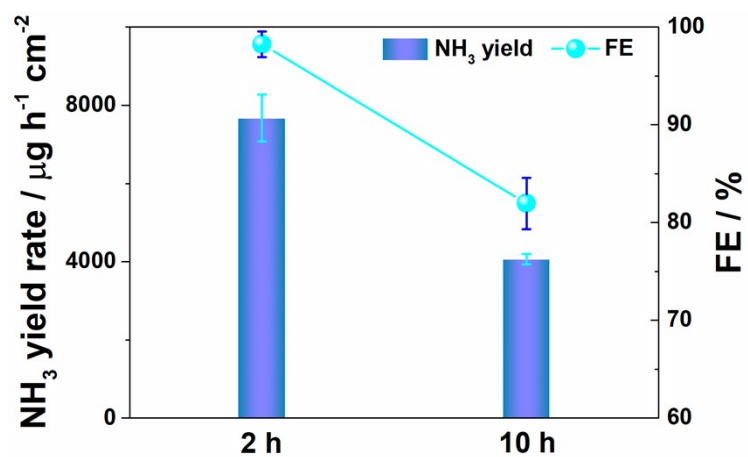


**Fig. S8** NH<sub>3</sub> yield rates and FEs of CF@Cu<sub>2</sub>O for NO<sub>2</sub><sup>-</sup>RR at different electrolysis time at -0.6 V vs. RHE.



**Fig. S9** Photograph of pH test with electrolyte before  $\text{NO}_2^-$ RR electrolysis.



**Fig. S10** Photograph of pH test with electrolyte after 2 h of  $\text{NO}_2^-$ -RR electrolysis.



**Fig. S11** Photograph of pH test with electrolyte after 10 h of  $\text{NO}_2^-$ -RR electrolysis.

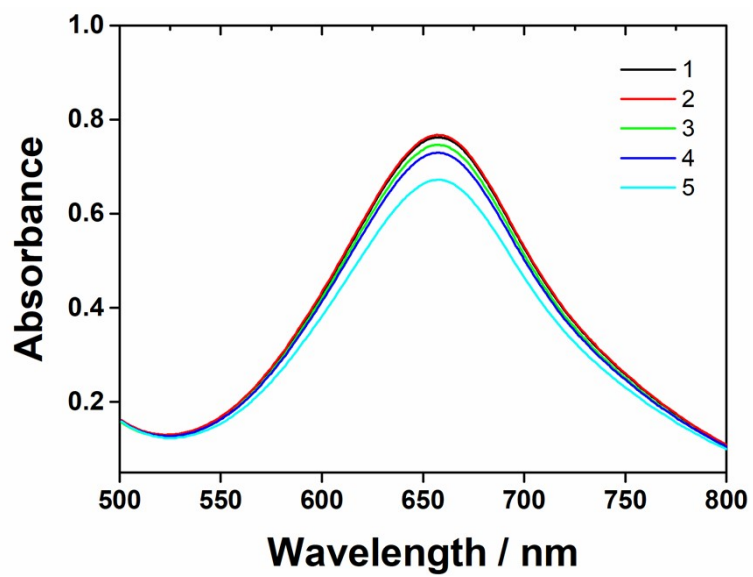


**Fig. S12** UV-Vis spectra of CF@Cu<sub>2</sub>O for NO<sub>2</sub><sup>-</sup>RR after continuous cycle tests at -0.6V vs RHE.

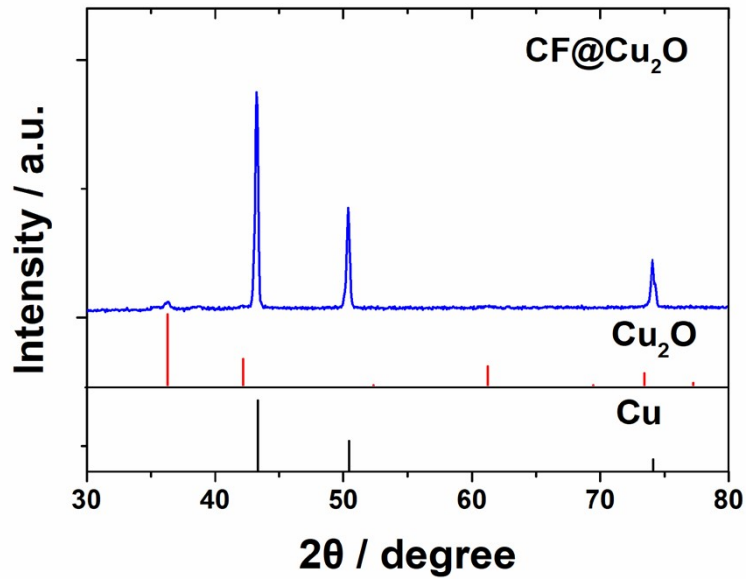
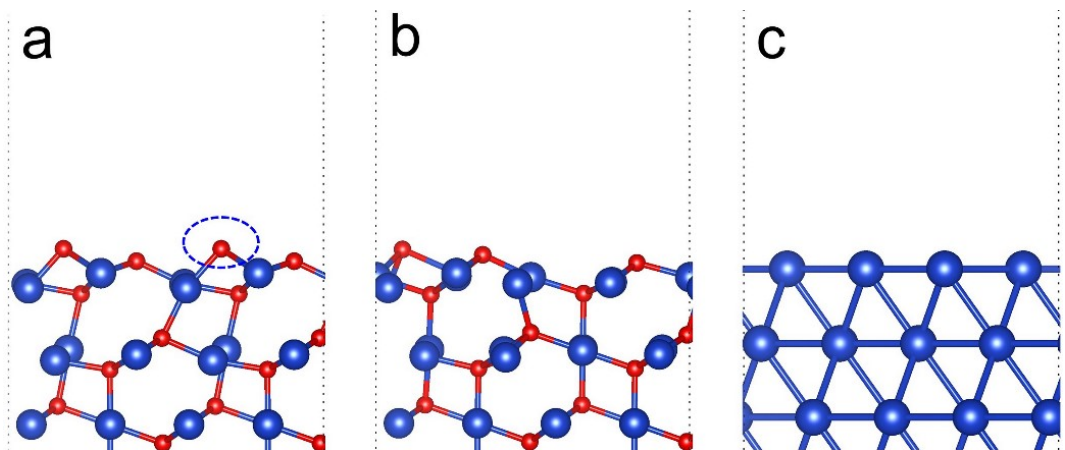
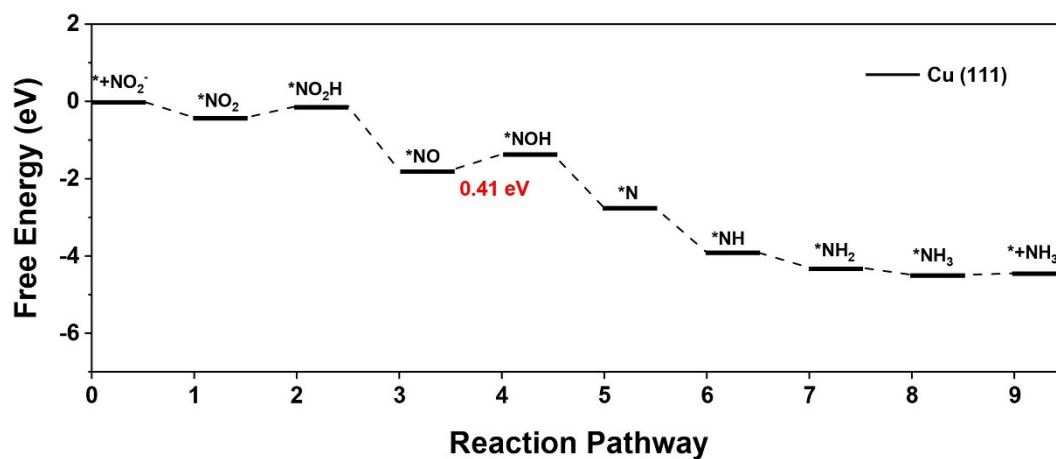


Fig. S13 XRD pattern of CF@Cu<sub>2</sub>O after continuous cycle tests.



**Fig. S14** Slab models of (a) pristine Cu<sub>2</sub>O (111), (b) Cu<sub>2</sub>O (111) with one OV, and (c) Cu (111) surfaces.



**Fig. S15** Free energy diagram of different intermediates generated during electrocatalytic NO<sub>2</sub><sup>-</sup>RR on the Cu (111).

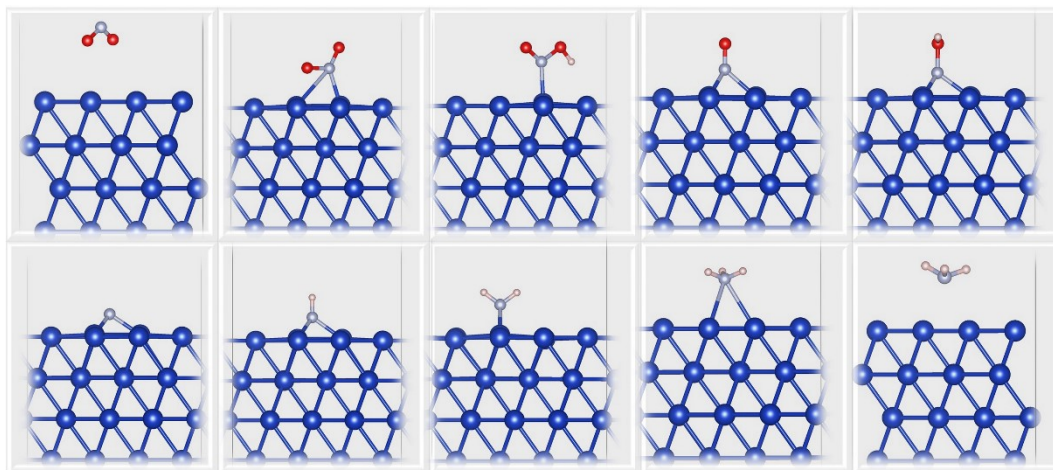


**Fig. S16** Optimized atomic configurations of the adsorbed intermediates on the Cu (111).

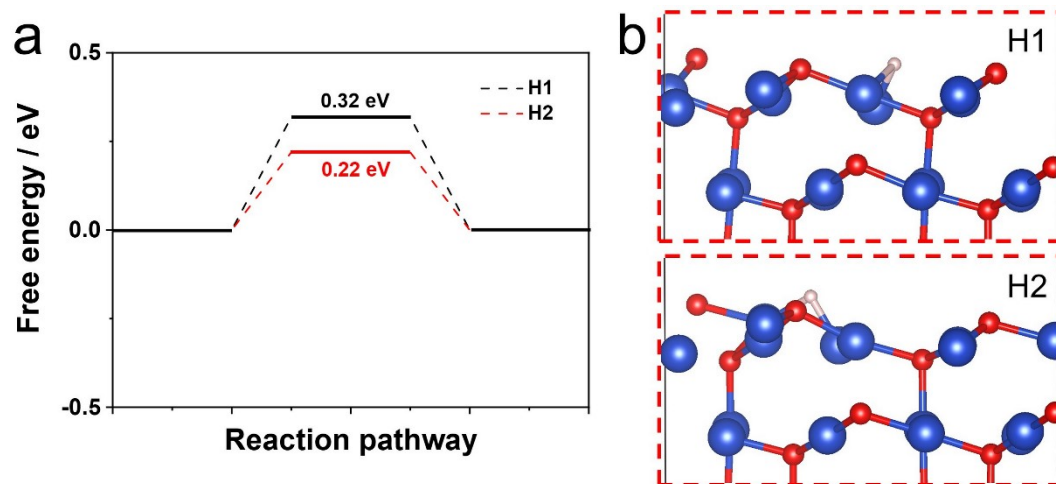


**Fig. S17** Free energy diagram of HER processing and corresponding atomic configurations on different site of Cu<sub>2</sub>O (111) with OVs.

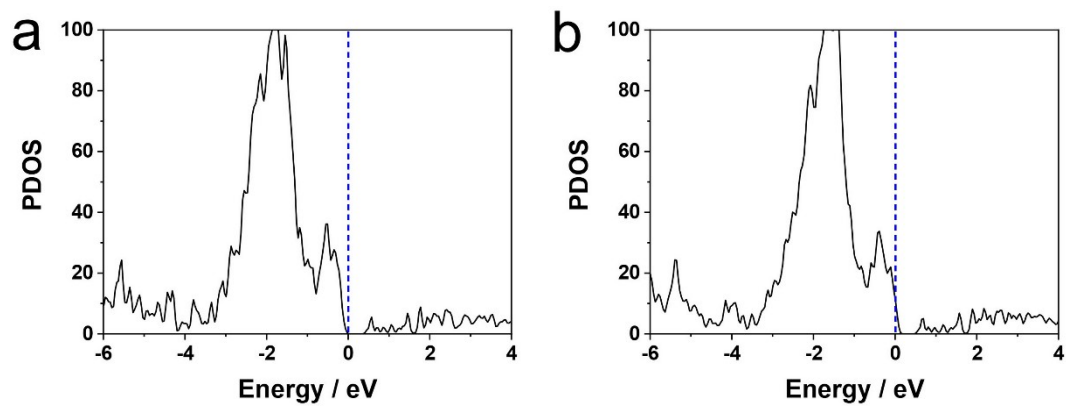


**Fig. S18** PDOS of pristine  $\text{Cu}_2\text{O}$  (111) (a) without and (b) with  $\text{NO}_2$  adsorption.

Fermi levels are set at 0 eV.

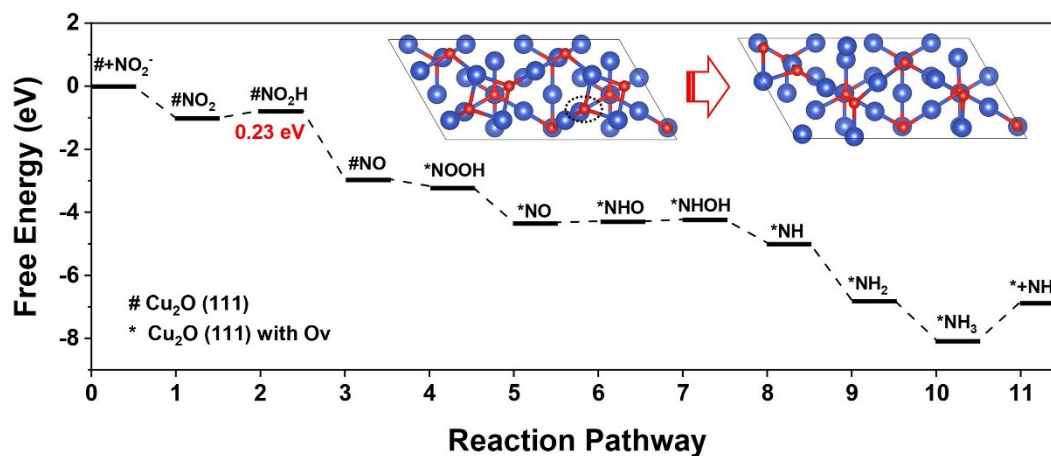


**Fig. S19** Free energy diagram of different intermediates generated during electrocatalytic NO<sub>2</sub>-RR on the Cu<sub>2</sub>O (111). The inset image illustrates the formation of OVs on the Cu<sub>2</sub>O (111) surface.

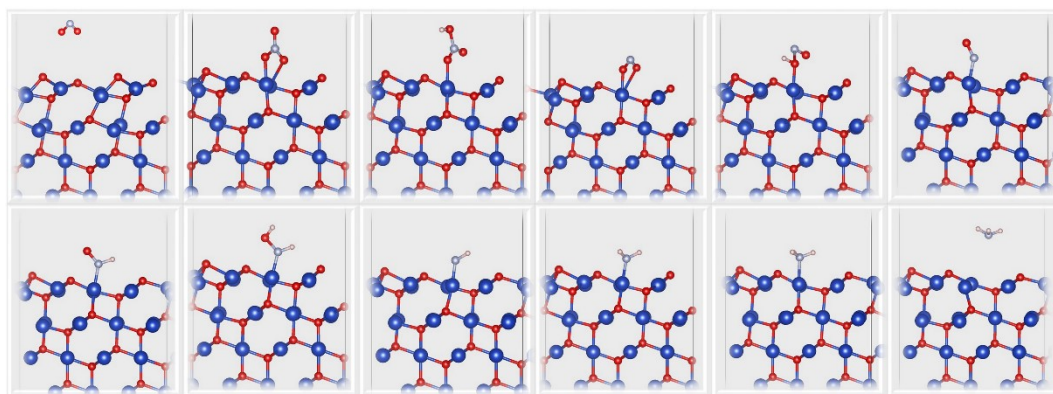


**Fig. S20** Optimized atomic configurations of the adsorbed intermediates on the  $\text{Cu}_2\text{O}$  (111).

**Table S1** Comparison of catalytic performance of CF@Cu<sub>2</sub>O with other reported NO<sub>2</sub><sup>-</sup>RR electrocatalysts.

Catalyst	Electrolyte	NH <sub>3</sub> yield rate	FE (%)	Ref.
<b>CF@Cu<sub>2</sub>O</b>	<b>0.1 M PBS + 0.1 M NaNO<sub>2</sub></b>	<b>7510.73 μg h<sup>-1</sup> cm<sup>-2</sup> (441.8 μmol cm<sup>-2</sup> h<sup>-1</sup>)</b>	<b>94.2</b>	<b>This work</b>
Cu phthalocyanine complexes	0.1 M KOH + 0.1 mM NaNO <sub>2</sub>	—	78.0	J. Appl. Electrochem., 1997, 27, 975–981.
Cobalt (II) porphyrazine	0.5 M NaOH + 0.0028 M NaNO <sub>2</sub>	37.1 μmol cm <sup>-2</sup> h <sup>-1</sup>	97.0	J. Electroanal. Chem., 1999, 27, 126-135
Poly-NiTRP complex	0.1 M NaClO <sub>4</sub> + 0.01 M NaNO <sub>2</sub>	c(NH <sub>3</sub> ) = 1.1 mM	—	Electrochim. Acta., 2011, 56, 5230–5237.
Cu <sub>80</sub> Ni <sub>20</sub>	1.0M NaOH + 20 mM NaNO <sub>2</sub>	—	87.6	Electrochim. Acta, 2013, 89, 488–496.
MoFe protein	0.25 M HEPES buffer +0.05 M NO <sub>2</sub> <sup>-</sup>	0.468 μmol cm <sup>-2</sup> h <sup>-1</sup>	~100	Energy Environ. Sci., 2016, 9, 2550–2554
Co-tripeptide complex (CoGGH)	1.0 M NaNO <sub>2</sub> + 1.0 M MOPS	3.01 × 10 <sup>-10</sup> mol s <sup>-1</sup> cm <sup>-2</sup>	90±3	J. Am. Chem. Soc. 2018, 140, 16888–16892.
MnO <sub>2</sub> nanoarrays	0.1M Na <sub>2</sub> SO <sub>4</sub> + 4 mM NaNO <sub>2</sub>	3.09 × 10 <sup>-11</sup> mol s <sup>-1</sup> cm <sup>-2</sup>	6.0	Chem. Commun., 2018, 54, 10340–10342.
Oxo-MoS <sub>x</sub>	0.1 M nitrite in 0.2 M citric acid (pH = 5)	—	13.5	J. Am. Chem. Soc. 2018, 140, 2012–2015
Rh/Al <sub>2</sub> O <sub>3</sub>	25 mM phosphate Buffer +50 mM NO <sub>2</sub> <sup>-</sup>	—	~68–95	ACS Catal., 2020, 10, 494–509
Cu <sub>x</sub> Ir <sub>1-x</sub>	0.1 M phosphate buffer +100 ppm NO <sub>2</sub> <sup>-</sup>	—	~100	ACS Catal., 2020, 10, 7915–7921
FeN <sub>5</sub> H <sub>2</sub>	1.0 M MOPS + 1.0 M NaNO <sub>2</sub>	—	> 90	ACS Catal., 2020, 10, 13968–13972
Ni-NSA-V <sub>Ni</sub>	0.2 M Na <sub>2</sub> SO <sub>4</sub> + 200 ppm NO <sub>2</sub> <sup>-</sup>	235.98 μmol h <sup>-1</sup> cm <sup>-2</sup>	88.9	J. Mater. Chem. A, 2021, 9, 239–243
GCC-CoDIM	0.5 M Na <sub>2</sub> SO <sub>4</sub> + 20 mM NaNO <sub>2</sub>	—	99.5	J. Am. Chem. Soc., 2021, 143, 7203–7208
Cu <sub>3</sub> P NA/CF	0.1 M PBS + 0.1 M NO <sub>2</sub> <sup>-</sup>	1626.6 μg h <sup>-1</sup> cm <sup>-2</sup>	91.2 ± 2.5	Green. Chem., 2021,23, 5487–5493

## References

1. P. Searle, *Analyst*, 1984, **109**, 549–568.
2. G. Kresse and J. Furthmüller, *Phys. Rev. B*, 1996, **54**, 11169–11186.
3. G. Kresse and D. Joubert, *Phys. Rev. B*, 1999, **59**, 1758–1775.
4. J. Perdew, K. Burke and Y. Wang, *Phys. Rev. B*, 1996, **54**, 16533–16539.
5. J. Perdew, K. Burke and M. Ernzerhof, *Phys. Rev. Lett*, 1996, **77**, 3865–3868.
6. S. Grimme, *J. Comput. Chem.*, 2004, **25**, 1463–1473.
7. S. Grimme, *J. Comput. Chem.*, 2006, **27**, 1787–1799.
8. V. Wang, N. Xu, J. Liu, G. Tang and W. Geng, *Comput. Phys. Commun.*, 2021, **267**, 108033.